Radiation Physics and Chemistry 176 (2020) 108809

Contents lists available at ScienceDirect

Radiation Physics and Chemistry

journal homepage: www.elsevier.com/locate/radphyschem

Experimental and theoretical L-shell ionization cross sections of heavy atoms by impact of Si ions

M. Oswal[a,b], Sunil Kumar[b,c], Udai Singh[d], Shashank Singh[b], G. Singh[e], K.P. Singh[b], D. Mehta[b], A.M.P. Mendez[f], D.M. Mitnik[f], C.C. Montanari[f], D. Mitra[g], T. Nandi[h,*]

[a] Department of Physics, Dev Samaj College, Sec 45-B Chandigarh 160047, India
[b] Department of Physics, Panjab University, Chandigarh 160014, India
[c] Govt. Degree college, Banjar,Kullu (HP) 175123, India
[d] The Marian Smoluchowski Institute of Physics, Jagiellonian University, Lojasiewicza 11, 30-348 Krakow, Poland
[e] Department of Physics, Punjabi University, Patiala, Punjab-147002, India
[f] Instituto de Astronomía y Física del Espacio, CONICET and Universidad de Buenos Aires, Buenos Aires, Argentina
[g] Department of Physics, Kalyani University, Kalyani (WB) 741235, India
[h] Inter-University Accelerator Centre, JNU New Campus, New Delhi110067, India

ARTICLE INFO

Keywords:
L-shell x-rays
Heavy ions
Ionization
Multiple-ionization

ABSTRACT

We present a theoretical and experimental study of the subshell resolved L-shell ionization of relativistic targets such as $_{73}$Ta, $_{78}$Pt, $_{90}$Th, and $_{92}$U. The measurements of x-ray production cross sections by (84–140 MeV) Si^{+q} ions (q = 8; 12), were held at the Inter-University Accelerator Centre of New Delhi. Multiple-hole fluorescence and Coster-Kronig yields were used to obtain the L_i(i = 1–3) ionization cross sections from the measured x-ray production cross sections of *Lℓ*, *Lα*, and *Lβ*, *Lη*, and *Lγ* lines. The experimental results are compared with *ab initio* theoretical calculations by means of the *shell-wise local plasma approximation* (SLPA). This model uses the quantum dielectric formalism to obtain the total ionization cross sections from an initial ground state. The wave functions and binding energies of the different targets were obtained by solving the fully relativistic Dirac equation using the HULLAC code package. These calculations are based on first order perturbation theory with a central field, including Breit interaction and quantum electrodynamics corrections. The present SLPA ionization cross sections of the L-shell are found to be independent of the charge state of the Si ions. The experimental observations display also quite similar character if the correct mean projectile charge state inside the target is used for including the multiple ionization effect during ion-solid collisions. A general good agreement between the experimental measurements and full theoretical calculations supports the reliability of present results. The comparison also includes the well-known ECPSSR and ECUSAR semi empirical approximations. We noted that the ECUSAR results agree well with the SLPA, while the ECPSSR cross sections are rather low.

1. Introduction

Accurate determination of the x-ray production cross sections is important because of their wide use in the fields of atomic and molecular physics (Satoh, 2015; Sharma and Nandi, 2016; Dyson, 1990), and non-destructive elemental analysis of materials. Reliable values of L-shell ionization cross sections are included in the extended particle induced x-ray emission technique (PIXE) (Antoszewska-Moneta et al., 2015; Gillespie et al., 2015). Since the inception, PIXE mostly uses light ions such as protons or alphas (Johansson et al., 1970; GARCIA et al., 1973) but an increasing interest is being noticed in using heavy ions due to the higher cross sections and hence, better sensitivity (Richard, 1975).

Ionization cross sections have been subject of theoretical developments since the very beginning of the atomic physics up to the present (Beyer and Shevelko, 1999; Montanari and Miraglia, 2017b; Lapicki, 2002), covering from the first order plane-wave approximations (Brandt and Lapicki, 1981) to the non-perturbative distorted-waves (Crothers and McCann, 1984), the independent electron approximations, or the density-dependent models (Montanari et al., 2011). In relation to PIXE, the principal source of theoretical cross sections is the ECPSSR by Lapicki and coworkers, and further developments of this model (Lapicki, 2002; Brandt and Lapicki, 1979, 1981). However, the disagreement between the experimental and theoretical cross sections is

* Corresponding author.
E-mail address: nanditapan@gmail.com (T. Nandi).

https://doi.org/10.1016/j.radphyschem.2020.108809
Received 1 October 2018; Received in revised form 20 February 2020; Accepted 21 February 2020
Available online 27 February 2020
0969-806X/ © 2020 Elsevier Ltd. All rights reserved.

still a subject of concern. Discrepancies between the theories and experiments are partially ascribed to the fluorescence yields, the Coster-Kronig transitions (CK), and the correct inclusion of the multiple ionization (Lapicki et al., 2004; Naga Raju et al., 2004).

The aim of this work is to present reliable values of L-subshell ionization cross sections by comparing new measurements with a full theoretical description: the shell-wise local plasma approximation (SLPA) (Montanari et al., 2011; Montanari and Miraglia, 2013). The SLPA is an *ab initio* theory in which the only input required are the wave functions and the binding energies of the electrons in the target initial state. In a recent paper (Oswal et al., 2018) we used the SLPA to compare with measured L x-ray production cross sections of W, Au, Bi and Pb, based on (Montanari et al., 2011). In the present work, we extended the investigation to other many-electron targets: $_{73}$Ta, $_{78}$Pt, $_{90}$Th, and $_{92}$U. This requires new developments to describe the wave functions and binding energies. The study of these relativistic targets provides also an opportunity to evaluate future possibilities of generating effective potentials, in order to describe the different subshells. The unique potential enables one to represent bound and continuum states on the same footing, being of great interest for inelastic collisional calculations. That could be useful not only within the SLPA, but also in other approaches such as the Continuum-Distorted Wave-Eikonal-Initial-State (CDW-EIS) theory.

We present here new data and theoretical results for the subshell resolved L-shell ionization cross sections by impact of ^{28}Si ions (charge states 8^+ and 12^+) in the energy range 84–140 MeV. With a projectile nucleus $Z_P = 14$ and high Z_T targets, the present collisional systems are highly asymmetric $0.15 \leq Z_P/Z_T \leq 0.19$. At high impact energies, the L x-ray production cross sections are mainly due to ionization, with capture being important at intermediate to low energies. The experimental-theoretical comparison presented here also includes the ECPSSR and ECUSAR approximation results, which represent a general reference in the field.

The paper is organized as follow. In section II, the details of the experimental setup and the data analysis are presented. In section III we summarize the SLPA and give details about the present theoretical aspects involving the calculation of the relativistic targets structure, and their binding energies. In Section IV we discuss the single- and multiple-hole atomic parameters required for the conversion of the x-ray production cross sections to ionization cross sections. Section V summarizes the results and finally, conclusions are presented in section VI.

2. Experimental details and data analysis

The L x-ray production cross-sections have been measured using the 15 UD Pelletron accelerator at Inter-University Accelerator Centre (IUAC), New Delhi. Details of the experimental setup are given in Kumar et al. (Kumar et al., 2017). Spectroscopically, pure (99.999%) thin targets of $_{73}$Ta (166 μg/cm^2), $_{90}$ThF$_4$ (48.7 μg/cm^2), $_{92}$UF$_4$ (48.6 μg/cm^2) on Mylar backing (of thickness $\sim$ 3 μm) and $_{78}$Pt (120 μg/cm^2) on carbon backing (of thickness $\sim$ 20 μg/cm^2) were used in the present work. A Si(Li) solid state detector (thickness = 5 mm, diameter = 10 mm, 25 µm Be window from ORTEC, Oak Ridge, Tennessee, USA) was used to detect the x-rays. Background subtracted L x-ray spectra of $_{73}$Ta, $_{78}$Pt, $_{90}$Th and $_{92}$U for 140 MeV ^{28}Si ions are shown in Fig. 1.

The recorded spectra exhibit peaks corresponding to the ionized L_i (i = 1, 2, 3) subshells. From the recorded spectrum, it is clear that at least six different L x-ray lines are resolved and the separation between different peaks increases with the increase of Z of the target.

The spectra were analyzed with multi-Gaussian least-squares-fitting program with the possibility of choosing variable widths of the lines and linear background subtraction. A typical fitted spectrum for $_{73}$Ta target bombarded with 140 MeV ^{28}Si beam is shown in Fig. 2.

All the L x-ray lines along with their origin are labeled in the spectrum shown in Fig. 2. This spectrum in semi-log plot shows weak appearance of Lη line also. The exponential background is also shown in Fig. 2 with a dashed-line. The ratios of net counts to the background are 0.26, 0.0321, 0.026, and 0.080 for Ll, Lα, Lβ, and Lγ, respectively.

The L x-ray production cross section, $\sigma_i^x(E)$ of the ith· x-ray line at the incident projectile energy E, is calculated using the following relation:

$$\sigma_i^x = \frac{Y_i^x\ A\ Sin\theta}{N_A \varepsilon n_p\ t\ \ \beta} \tag{1}$$

where Y_i^x is the intensity of the i^{th}x-ray peak, A is the atomic weight of the target, θ is the angle between the incident ion beam and the target foil normal, N_A is the Avogadro number, n_p is the number of incident projectiles, ε is the effective efficiency of the x-ray detector, t is the target thickness in µg/cm^2 and $\beta \equiv [1 - \exp(-\mu t)]/\mu t$ is the correction factor for the absorption of the emitted L x-rays inside the target, where µ in cm^2/µg is the attenuation coefficient.

Number of the projectile ion n_p are obtained from the ratio of the total charge collected in a Faraday cup and the mean charge state of the projectile evaluating from the ETACHA code (Lamour et al., 2015). The target of Ta, ThF_4 and UF_4 have been procured from NIST, so their thicknesses are taken as mentioned by the manufacturer. Whereas, the Pt target is prepared in the target lab of IUAC, New Delhi and the accurate thickness was measured using alpha scattering method. The attenuation coefficients µ are taken from the NIST XCOM program available online (https://physics.nist.gov/).

The effective efficiency ε, which includes the geometrical factor, absorption in the Mylar foil used in the window of the scattering chamber and the intrinsic efficiency of the detector, was measured carefully in the same geometry as used in the actual measurement. Details of the experimental technique for measuring effective efficiency are given in Kumar et al. (Kumar et al., 2017). Several low Z targets were used for producing the necessary K x-rays. The effective efficiency curve is obtained by measuring the K x-ray yields and compared it with the theoretical x-ray production cross sections. Measured values were normalized to obtain the absolute efficiency using the calibrated ^{137}Cs and ^{155}Eu radioactive sources. The efficiency values obtained in this manner are shown in Fig. 3. The energy calibration of the detector was performed before and after the measurements using the radioactive ^{55}Fe, ^{57}Co and ^{241}Am sources.

The percentage error in the measured x-ray production cross sections is about 10–12%. This error is attributed to the uncertainties in different parameters used in the analysis, namely, the photopeak area evaluation ($\leq$1% for the L$_\alpha$ x-ray peak and $\sim$ 3% for the other peaks), the ion beam current ($\sim$ 5%), and the target thickness ($\sim$ 3%). The error in the effective efficiency values, ε, is 5–8% in the energy region of current interest.

3. The relativistic calculation and the SLPA

The SLPA (Montanari et al., 2011; Montanari and Miraglia, 2013) is an *ab initio* approach for the calculation of ionization probabilities. It is based on the quantum dielectric response theory and needs as an input both the wave functions and binding energies of the target ground state. This model has been successfully employed to describe the different moments of the energy loss of ions in matter, i.e. ionization cross sections (moment zero) (Montanari et al., 2011; Kadhane et al., 2003), mean energy loss or stopping power (moment one) (Cantero et al., 2009; Montanari and Miraglia, 2017a), and energy loss straggling (moment two) (Montanari and Miraglia, 2013). Within the SLPA, the ionization cross section σ_q^j of the j-subshell due to the interaction with a projectile of impact velocity v, nuclear charge Z_P, N bound electrons and charge state $q = Z_P - N$, is expressed as

$$\sigma_q^j = \frac{2}{\pi\ v^2} \int_0^\infty [Z_P(q,\ k)]^2 dk \int_0^{k\ v} d\omega \int Im\left[\frac{-1}{\varepsilon_j(k,\ \omega,\ E_j,\ \delta_j\ (r))}\right] d\vec{r}. \tag{2}$$

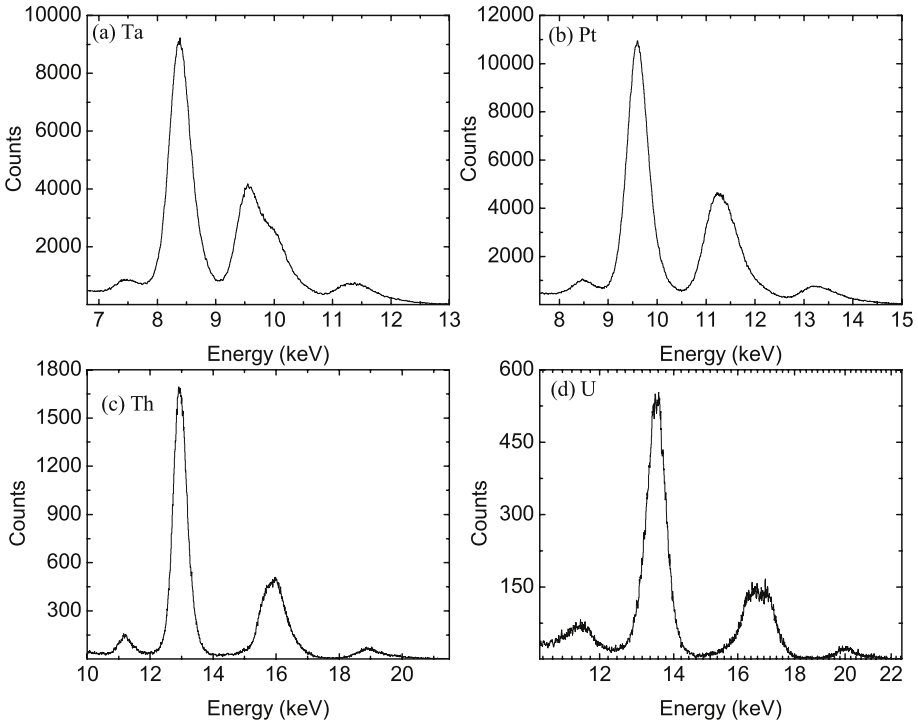

Fig. 1. L x-ray spectra of $_{73}$Ta, $_{78}$Pt, $_{90}$Th and $_{92}$U bombarded with the 107 MeV ^{28}Si ions.

The Levine-Louie dielectric function (Levine and Louie, 1982) is employed in $Im\left[\frac{-1}{\varepsilon_j(k,\omega,E_j,\delta_j)}\right]$, which depends on the moment and energy transferred to the target electrons, k and ω, and on the binding energies and density of electrons around the nucleus E_j and $\delta_j(r)$. The latters are the only inputs for our calculations. The ion (the nucleus screened by the bound electrons) is described as a not homogeneous effective charge $Z_P(q, k)$. For Si^{+12} and Si^{+8} we obtained $Z_P(q, k)$ from the tabulated Hartre-Fock wave functions of positive ions (Clementi and Roetti, 1974) (see the appendix of (Montanari et al., 2011) for details).

In the case of targets with high atomic number Z > 54, we must calculate the atomic structure by solving the relativistic Dirac equation instead of the Schrödinger equation. Previous calculations performed with non-relativistic or semi-relativistic approaches show large discrepancies with the experimental binding energies of the most tightly bound inner orbitals, enforcing to perform the calculations in a fully relativistic framework. To this end, we used the HULLAC code package (Oreg et al., 1991; Bar-Shalom et al., 2001), which allows us to obtain accurate relativistic orbitals and energies of the bound states. The calculations are based on first order perturbation theory with a central field. In this approach, an analytical parametric potential (Klapisch, 1971) given as a function of screening charge distribution, is generated and optimized, minimizing the first order energies of a given set of configurations. The calculations include the contributions from the Breit interaction and quantum electrodynamics corrections. Although this code was written for calculations of highly charged ions, it can be successfully employed in other atomic systems, such as the ones

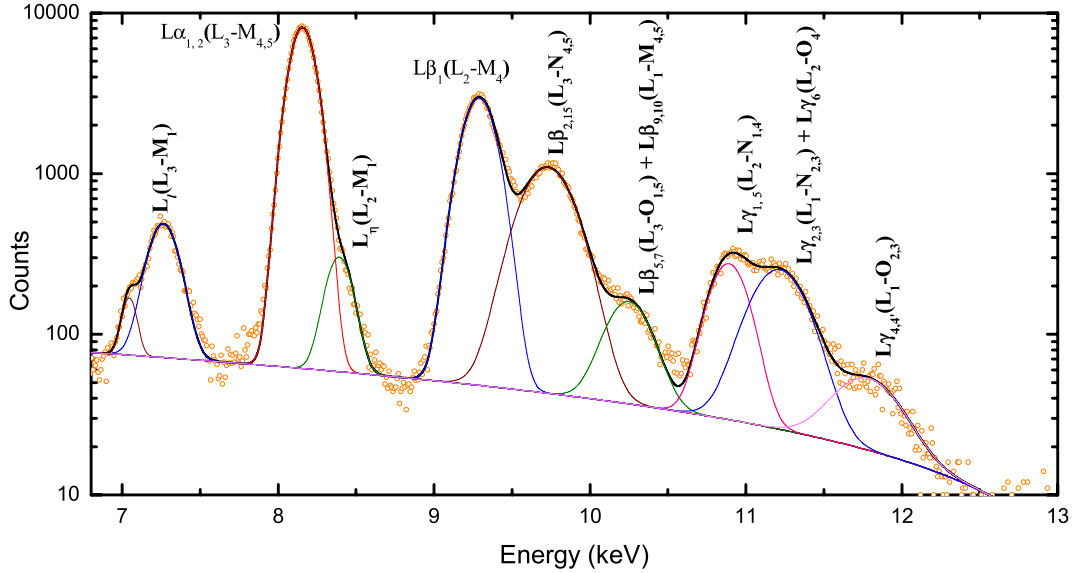

Fig. 2. L x-ray spectra of $_{73}$Ta bombarded with the 140 MeV ^{28}Si ions. Deconvoluted X-ray lines due to different transitions are shown along with the background due to Compton scattering.

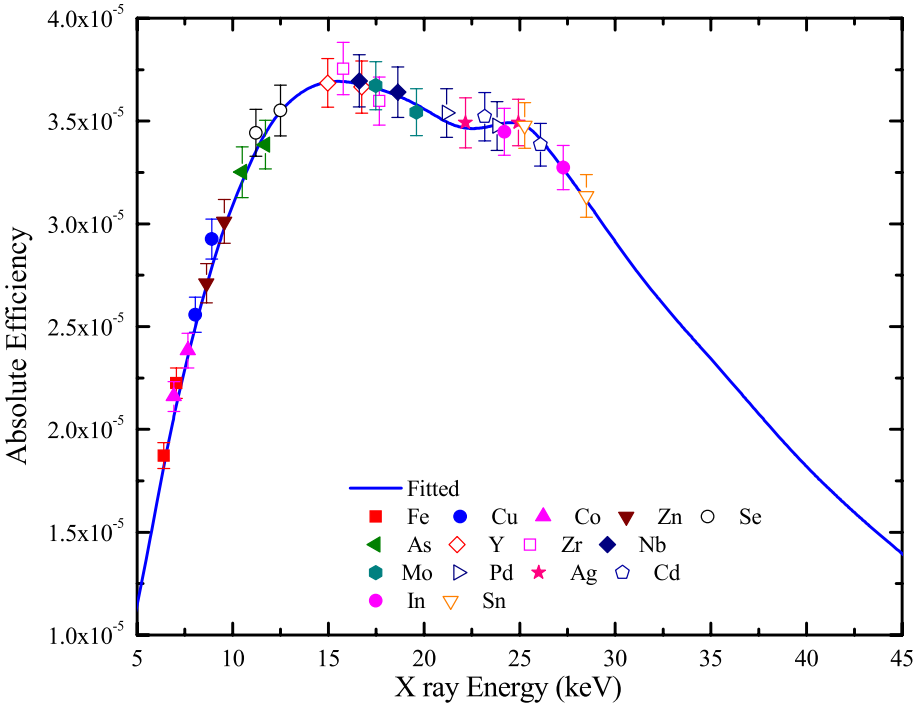

Fig. 3. Efficiency curve obtained by measuring the K x-rays fluorescence yields from targets excited by the 59.54 keV γ-ray photons. Measured values were normalized to absolute efficiency obtained using the calibrated ^{137}Cs and ^{155}Eu radioactive sources.

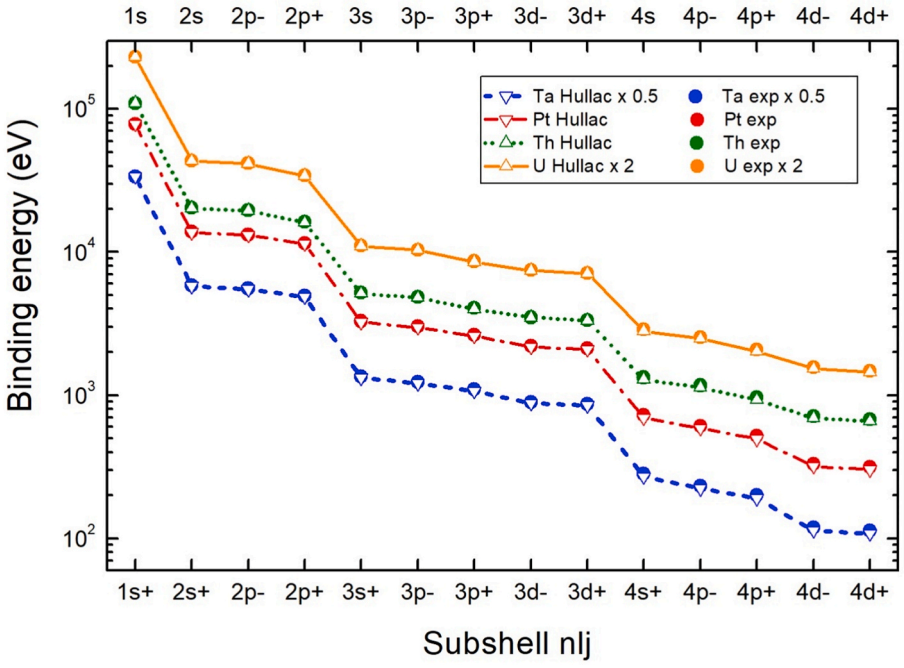

Fig. 4. Binding energies for the bound electrons in Ta, Pt, Th and U. Present relativistic results are compared with the experimental values (Williams, 1992).

presented here. In this way, we calculated the E_j and $\delta_j(r)$ to be included in Equation (2). The binding energies involved in the present work for $_{73}$Ta, $_{78}$Pt, $_{90}$Th, and $_{92}$U are obtained using the fully relativistic method and are shown in Fig. 4. The figure also includes the experimental binding energies compiled by (Williams, 1992). The values computed for the L-orbitals agree with the experimental ones within 1.5%, being less than 4% for the M and N-orbitals. The standard transition energies (Deslattes et al., 2003) following single vacancy of the L_i subshells are given in the Table 1 for the four elements studied here. We also include our relativistic results in Table 1. These values agree within 1%, and suitably describe the L x-ray spectra in Figs. 1 and 2.

4. Effect of single- and multiple-ionization on the conversion of x-ray production cross sections to ionization cross sections

The L x-ray production cross sections for the most commonly resolved $L\ell$, $L\alpha$, $L\beta$, $L\eta$, and $L\gamma$ x rays are related to the L_i(i = 1,2,3) subshell ionization cross sections as given below (Kumar et al., 2017)

Table 1
Energies of the L x-ray fluorescence transitions for the Ta, Pt, Th and U, the present relativistic calculations (see Section III) and the standard experimental values (Stand).

Fluorescence transition (subshell)	x-ray energy (keV)							
	$_{73}$Ta		$_{78}$Pt		$_{90}$Th		$_{92}$U	
	Relat	Stand	Relat	Stand	Relat	Stand	Relat	Stand
Lℓ (L_3)	7.174	7.173	8.268	8.268	11.118	11.118	11.618	11.618
Lα_1 (L_3)	8.146	8.117	9.442	9.402	12.967	12.890	13.615	13.527
Lα_2 (L_3)	8.088	8.117	9.362	9.402	12.809	12.890	13.438	13.527
Lη (L_2)	8.429	8.428	9.977	9.975	14.509	14.510	15.399	15.399
Lβ_1 (L_2)	9.343	9.345	11.071	11.062	16.200	16.146	17.219	17.152
Lβ_3 (L_1)	9.487	9.345	11.234	11.062	16.425	16.146	17.457	17.152
Lβ_4 (L_1)	9.213	9.345	10.854	11.062	15.641	16.146	16.576	17.152
Lβ_2 (L_3)	9.669	9.645	11.251	11.242	15.624	15.606	16.430	16.407
Lβ_{15} (L_3)	9.708	9.645	11.233	11.242	15.586	15.606	16.387	16.407
Lγ_1 (L_2)	10.963	10.895	12.942	12.942	18.978	18.983	20.167	20.167
Lγ_5 (L_2)	10.588	10.895	12.550	12.942	18.363	18.983	19.507	20.167
Lγ_2 (L_1)	11.232	11.380	13.273	13.487	19.305	19.701	20.487	20.920
Lγ_3 (L_1)	11.294	11.380	13.362	13.487	19.504	19.701	20.714	20.920

Table 2
There commended fluorescence and CK yields for singly ionized elements used in the present work (Rec) (Chen et al., 1981; Campbell, 2003), and compared to Krause (1979) and DHS (Scofield, 1974) values. Fractional radiative emission rates (Campbell and Wang, 1989) used here are also tabulated.

Fluorescence yield									
	ω_1			ω_2			ω_3		
Element	Rec.	DHS	Krause	Rec.	DHS	Krause	Rec.	DHS	Krause
$_{73}$Ta	0.145	0.131	0.137	0.280	0.28	0.258	0.251	0.251	0.243
$_{78}$Pt	0.130	0.074	0.114	0.344	0.344	0.321	0.303	0.303	0.306
$_{90}$Th	0.170	0.139	0.161	0.503	0.503	0.479	0.424	0.424	0.463
$_{92}$U	0.190	0.149	0.176	0.506	0.506	0.467	0.444	0.444	0.489
CK yield									
	f_{13}			f_{12}			f_{23}		
Element	Rec.	DHS	Krause	Rec.	DHS	Krause	Rec.	DHS	Krause
$_{73}$Ta	0.320	0.351	0.280	0.125	0.186	0.180	0.134	0.139	0.134
$_{78}$Pt	0.560	0.716	0.500	0.070	0.067	0.140	0.126	0.132	0.124
$_{90}$Th	0.660	0.659	0.570	0.060	0.058	0.090	0.103	0.106	0.108
$_{92}$U	0.670	0.660	0.570	0.035	0.051	0.080	0.140	0.139	0.167
Fractional radiative emission rates (Campbell and Wang, 1989)									
Element	$S_{\gamma 23,1}$ ($=\Gamma_{\gamma 2,3}/\Gamma_1$)			$S_{\gamma 15,2}$ ($=\Gamma_{\gamma 1,5}/\Gamma_2$)			$S_{\alpha 12,3}$ ($=\Gamma_{\alpha 1,2}/\Gamma_3$)		
$_{73}$Ta	0.1637			0.1639			0.8001		
$_{78}$Pt	0.1997			0.1697			0.7831		
$_{90}$Th	0.2021			0.1824			0.7485		
$_{92}$U	0.2021			0.1848			0.7749		

$$\sigma_{L1} = \frac{\sigma^x_{L\gamma 2+3}}{\omega_1 S_{\gamma 2+3,1}} \tag{3a}$$

$$\sigma_{L2} = \frac{\sigma^x_{L\gamma 1+5}}{\omega_2 S_{\gamma 1+5,2}} - \sigma_{L_1} f_{12} \tag{3b}$$

$$\sigma_{L3} = \frac{\sigma^x_{L\alpha}}{\omega_3 S_{\alpha\, 12,3}} - \sigma_{L_1}(f_{12} f_{23} + f_{13}) - \sigma_{L_2} f_{23} \tag{3c}$$

where $\sigma^x_{Lp}(p = \alpha, \gamma_{2+3}, \gamma_{1+5})$ are the x-ray production cross sections of the different L x-ray components, σ_{Li} $(i = 1\text{–}3)$ are the ionization cross sections for the L_i subshells (2s, $2p_{1/2}$, $2p_{3/2}$ respectively), ω_i $(i = 1\text{–}3)$ are the fluorescence yields, f_{ij} $(i < j)$ are the yields for the CK transition between the L_i and L_j subshells, and S_{pi} $(i = 1\text{–}3,\ p = \alpha, \gamma_{2+3}, \gamma_{1+5})$ are the fractional radiative emission rates.

The Lx-ray emission rates based on DHS calculation (Scofield, 1974) and the interpolated values using DF scheme by Campbell and Wang (1989) are available in the literature. For the two datasets of $S_{3\alpha}$, $S_{1\gamma}$ and $S_{2\gamma}$ values, the difference is 5–8% over the atomic range Z_T = 50–92, whereas, the other values differ from each other by less than 4%. We have used the most recent values from Campbell and Wang (1989) for the present analysis. The single-hole fluorescence ω_i^0 and CK yields f_{ij}^0 can be obtained from DHS (Scofield, 1974), Krause (1979) and Chen et al. (1981). The use of different sets of atomic parameters can change the x-ray production cross section by ~30%. Hence, recent values of ω_i^0 and f_{ij}^0 compiled by Campbell, 2003, 2009 for the elements with $25 \le Z \le 96$ have been used in the present work for singly-ionized atoms. A comparison of these recommended values and (Scofield, 1974; Krause, 1979) is displayed in Table 2.

As it is clear from the Fig. 2, that Lγ complex contains the transition

Table 3
Different charge states of ^{28}Si ion inside the bulk of the target (Nandi) (Nandi et al., 2018) and outgoing charge state from the target (Schiwietz) (Schiwietz and Grande, 2001).

Energy (MeV)	84	90	98	107	118	128	140
Nandi	12.95	12.99	13.03	13.07	13.11	13.15	13.18
Schiwietz	11.4	11.7	11.85	12	12.15	12.28	12.41

due to both $L_1(2s_{1/2})$ and $L_2(2p_{1/2})$ subshells. According to the set of equation (3), the production cross sections of the resolved constituents of L_γ line, along with the production cross sections of L_α peak containing the transition due to L_3 subshell can be used to obtain the ionization cross sections for all the three subshells. It is clear from Eq. (3a) that the $L_{\gamma 2,3}$ production cross section is needed to obtain the L_1 sub-shell ionization cross section. But due to the limited energy resolution of the x-ray detectors, the Lγ peak is resolved into 3 components (i.e. $L_{\gamma 1,5}$, $L_{\gamma 2,3,6}$ and $L_{\gamma 4,4'}$). To obtain the yield of the $L_{\gamma 2,3}$ line, the contribution from $L_{\gamma 6}$ peak must be subtracted from the experimentally obtained $L_{\gamma 2,3,6}$ one. From the ratio of the radiative transition probabilities (i.e. $\Gamma_{\gamma 6}/\Gamma_{\gamma 1,5}$) and the yield of the $L_{\gamma 1,5}$ line, the contribution of $L_{\gamma 6}$ can be estimated.

The uncertainties in the ionization cross sections are a bit larger due to the propagation of errors as per the set of equation (3). Error in fluorescence yield (Campbell, 2003, 2009) ω_1, which is used for finding the ionization cross section of L_1 subshell is 15% for $_{73}$Ta and 30–35% for the other elements. However, for ω_2 and ω_3 it is 5% for all the elements. Errors quoted in the literature (Campbell, 2003, 2009) for Coster-Kronig rates are as high as 15–50% for f_{12} and f_{13} and 5–10% f_{23} respectively. We are not considering the errors in fractional radiative width $S_{p,i}$ because it's a ratio of emission rates for electric dipole transitions. Considering all the uncertainties taken into account along with the uncertainties of x-ray production cross sections of required lines, the overall errors are estimated according to the rule of propagation of errors. In L_1 ionization cross section it is 15–20% for $_{73}$Ta and 30–35% for all other elements. However, for the L_2 and L_3 sub-shell the uncertainty is 12–15% for all the elements investigated here.

The multiple-ionization effect in L-shell ionization by heavy ions has been known since decades (Pajek et al., 2003; Singh et al., 2000). In the present work, single-hole fluorescence ω_i^0 and CK yields f_{ij}^0 (Chen et al., 1981), were corrected for multiple ionization using a model prescribed by Lapicki et al. (1986). The ionization probability $P(v_P)$ of an electron in a manifold of the outer subshells by a projectile with nuclear charge Z_P, charge state q and velocity v_P,can be calculated from equation (A3) of (Lapicki et al., 1986) as follows

$$P(v_P) = \frac{q^2}{2\beta v_P^2}\left(1 - \frac{\beta}{4v_P^2}\right) \tag{4}$$

with β = 0.9 (Mehta et al., 1993) and $q = q_e$, the equilibrium charge state of the ion in the bulk. The ion beam changes its charge state during its passage through the target. Till date, q_e has been obtained from empirical formulas, such as those by Schiwietz and Grande (2001), based on measurements by electromagnetic methods outside the solid. These measurements involve the ion charge state in the bulk and the changes due to the interaction with the solid surface. However, our experimental geometry concerns only to the charge state evolution of the ion in the bulk. In this scenario the mean charge state in the bulk is calculated using the method in (Nandi et al., 2018). The comparison between the mean charge states in the bulk (Nandi et al., 2018) and in the bulk plus surface (Schiwietz and Grande, 2001) is shown in Table 3. Considerable differences between them can be seen, with the former being always higher than the latter. It implies that electron capture processes take place at the solid surface. We can also observe in Table 3 that the equilibrium charge state of the Si ions is $q_e \approx 13$ for the four targets and impact energies considered here, and almost independent of initial charge state q.

The single-hole fluorescence and CK yields values ω_i^o and f_{ij}^o are corrected for ionization in outer subshells as follows

$$\omega_i(v) = \omega_i^o[1 - (1 - \omega_i^o)P(v)]^{-1}, \tag{5a}$$

$$f_{ij}(v) = f_{ij}^o(1 - P(v))^2, \tag{5b}$$

while the fractional rates F_{ip} considered to be remain unchanged (both partial and total non-radiative widths are narrowed by identical factors). With equation (5), the single-hole fluorescence and CK yields are changed at the different ion beam energies and charge states. The effect of multiple-ionization in the atomic parameters is shown in Table 4 for 107 MeV Si^{+8} ions in Ta, Pt, Th and U. It is clear from this table that the fluorescence yields ω_i are enhanced up to ~220% and CK yields f_{ij} are reduced up to ~85% from single-hole to multiple-hole atom. These values differ by 40% over the range of the ion beam energies and the projectile charge states used in the present experiment. These modified values of atomic parameters (i.e. ω_i and f_{ij}) were used to extract the ionization cross sections from measured x-ray production cross sections.

Table 4
The fluorescence and CK yields for the singly ionized (SI) (Chen et al., 1981; Campbell, 2003) and multiply ionized (MI) target elements at the 107 MeV $^{28}Si^{8+}$ ion beam used in the present work. The mean charge state inside the target is 13.07 that is used in equation (4), much higher than the incident charge state. Then equation (5) is used for obtaining the fluorescence and CK yields due to multiple ionization.

Atomic number (Z)		Fluorescence yield			CK yield		
		ω_1	ω_2	ω_3	f_{12}	f_{13}	f_{23}
73	SI	0.145	0.280	0.251	0.125	0.320	0.134
	MI	0.3040	0.5024	0.4652	0.0175	0.0487	0.0199
78	SI	0.130	0.344	0.303	0.070	0.560	0.126
	MI	0.2504	0.5765	0.5302	0.0111	0.0809	0.0187
90	SI	0.170	0.503	0.424	0.060	0.660	0.103
	MI	0.3292	0.7243	0.6565	0.0059	0.0920	0.0153
92	SI	0.190	0.506	0.444	0.035	0.670	0.140
	MI	0.3439	0.7267	0.6746	0.0052	0.0920	0.0208

5. Results and discussion

The main results of the present research are summarized in Table 5 and Figs. 5–8. The experimental L x-ray productions cross sections were turned into ionization cross sections using Equation (3), with the multiple-hole parameters obtained from Table 2 and the Equations (4) and (5). In Table 5 we show the experimental L_i ionization cross sections of $_{73}$Ta, $_{78}$Pt, $_{90}$Th, and $_{92}$U, together with the SLPA ab initio results at corresponding energies and incident charge states of the silicon ions. We complete the comparison by including the cross sections from ECPSSR, ECUSAR and first Born approximations (FBA) too. These values are also displayed in Figs. 5–8, except for the FBA because, as expected, the FBA cross sections are too high, and they are included in Table 5 only as an upper limit.

The theoretical calculations consider the different charge states of the Si ions as expressed in Eq. (2). However, the SLPA results show no evidence of the charge state effect in the calculated L-shell ionization cross sections. The theoretical values agree within 0.5% for the different ion charge states, i.e. q = +8, +12 and + 14. This 0.5% uncertainty is within the numerical integration error. However, we have used q~13, the mean charge state of the projectile in the bulk, in equation (4).

The new theoretical developments to obtain the different L_i ionization cross sections using the SLPA and the relativistic solutions for $_{73}$Ta, $_{78}$Pt, $_{90}$Th, and $_{92}$U are tested in two different ways, one with the experimental data and another with the semiempirical ECPSSR and

Table 5
L_i ionization cross section for Ta, Pt, Th, and U elements bombarded with ^{28}Si ions. In L_1 ionization cross section uncertainty is 15–20% for Ta and 30–35% for all other elements. For the L_2 and L_3 sub-shell the uncertainty is 12–15% for all the elements investigated here.

Element	^{28}Si ion beam		Ionization cross sections (barns/atom)				
	Energy (MeV)	Charge state	Experiment	SLPA	ECUSAR	ECPSSR	FBA
$_{73}$Ta							
***L*$_1$**	84	12.95	869	4088	2026	1957	14040
	90	12.99	1414	5228	2755	2744	16980
	98	13.03	1912	6962	3984	3999	21180
	107	13.07	3552	9205	5703	5691	26190
	118	13.11	10453	12270	8295	8163	32870
	128	13.15	13236	15370	10996	10795	38970
	140	13.18	13407	19410	14627	14438	46420
***L*$_2$**	84	12.95	4036	7379	6831	6576	24200
	90	12.99	5505	8798	8269	8002	27280
	98	13.03	7394	10870	10384	10034	31430
	107	13.07	8927	13380	13009	12499	36120
	118	13.11	20612	16680	16870	15770	44500
	128	13.15	25426	19890	20393	18989	49880
	140	13.18	32094	24020	24859	23162	56090
***L*$_3$**	84	12.95	13813	25690	24141	22950	78730
	90	12.99	18594	29660	28947	27688	87540
	98	13.03	24451	35140	35901	34310	99170
	107	13.07	30644	41670	44368	42175	111900
	118	13.11	71016	49930	56864	52383	136500
	128	13.15	84195	57800	67687	62233	150200
	140	13.18	98081	67680	81037	74769	165500
$_{78}$ Pt							
L1	84	12.95	419	1530	0818	0781	5681
	90	12.99	454	2085	1099	1070	7097
	98	13.03	243	2996	1599	1581	9196
	107	13.07	527	4209	2346	2329	11800
	118	13.11	1928	5889	3541	3490	15330
	128	13.15	5706	7628	4857	4781	18690
	140	13.18	9845	9893	6716	6628	22890
L2	84	12.95	2154	3167	3213	3133	11830
	90	12.99	2621	3870	3920	3837	13480
	98	13.03	3842	4870	4971	4860	15750
	107	13.07	5265	6116	6293	6124	18380
	118	13.11	9918	7799	8218	7832	22700
	128	13.15	10216	9431	10054	9541	25880
	140	13.18	13402	11580	12436	11790	29660
L3	84	12.95	8233	14780	12484	12026	42670
	90	12.99	9819	17180	15072	14595	47930
	98	13.03	13397	20570	18866	18247	55030
	107	13.07	18352	24550	23562	22667	63020
	118	13.11	34094	29710	30431	28516	77120
	128	13.15	39009	34610	36685	34260	86200
	140	13.18	50632	40770	44592	41690	96680
$_{90}$Th							
L1	84	12.95	0092	0101	0162	0157	0546
	90	12.99	0146	0148	0186	0170	0705
	98	13.03	0052	0243	0234	0214	0979
	107	13.07	0063	0390	0315	0301	1370
	118	13.11	0392	0617	0468	0460	2000
	128	13.15	0465	0887	0659	0657	2650
	140	13.18	1800	1280	0964	0956	3570
L2	84	12.95	0418	0402	0579	0573	2150
	90	12.99	0523	0508	0718	0712	2520
	98	13.03	0764	0685	0929	0921	3040
	107	13.07	1186	0922	1202	1188	3660
	118	13.11	1886	1250	1593	1561	4560
	128	13.15	2408	1560	1989	1944	5370
	140	13.18	2598	2000	2519	2459	6380
L3	84	12.95	2057	3140	2959	2906	10600
	90	12.99	2611	3790	3613	3562	12200
	98	13.03	3461	4720	4592	4522	14300
	107	13.07	5275	5810	5832	5722	16900
	118	13.11	8746	7300	7613	7358	20700
	128	13.15	10893	8760	9353	9009	23800
	140	13.18	13214	10600	11636	11194	27600

(*continued on next page*)

Table 5 (*continued*)

Element	^{28}Si ion beam			Ionization cross sections (barns/atom)			
	Energy (MeV)	Charge state	Experiment	SLPA	ECUSAR	ECPSSR	FBA
$_{92}$U							
L1	84	12.95	0005	0053	0136	0132	0381
	90	12.99	0075	0079	0152	0138	0484
	98	13.03	0210	0132	0184	0167	0667
	107	13.07	0155	0212	0239	0227	0938
	118	13.11	0806	0355	0346	0339	1383
	128	13.15	1082	0518	0481	0480	1865
	140	13.18	1200	0766	0702	0697	2549
L2	84	12.95	0392	0280	0442	0438	1623
	90	12.99	0420	0369	0550	0545	1908
	98	13.03	0577	0495	0713	0707	2315
	107	13.07	0851	0655	0925	0916	2807
	118	13.11	1290	0902	1230	1208	3507
	128	13.15	1578	1160	1540	1509	4145
	140	13.18	2253	1484	1957	1915	4951
L3	84	12.95	1888	2424	2387	2348	8589
	90	12.99	2157	2915	2920	2881	9867
	98	13.03	3164	3654	3716	3665	11650
	107	13.07	4258	4573	4729	4648	13747
	118	13.11	7343	5743	6180	5993	16897
	128	13.15	8878	6914	7609	7354	19492
	140	13.18	11561	8437	9490	9160	22670

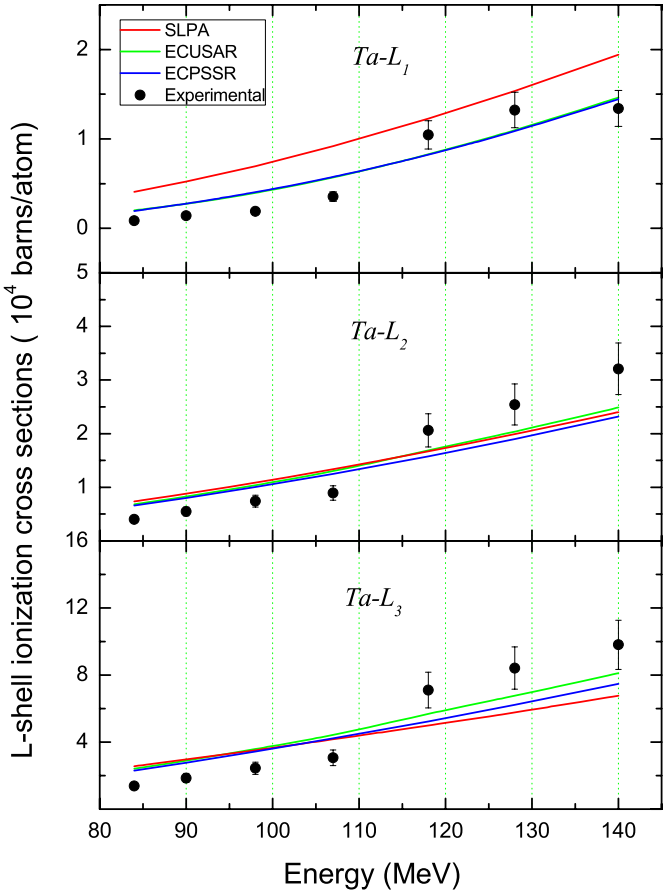

Fig. 5. Comparison of the experimental L_1, L_2, L_3 ionization cross sections for Ta induced by Si ions with different theoretical predictions: SLPA, ECUSAR, ECPSSR (details in the inset).

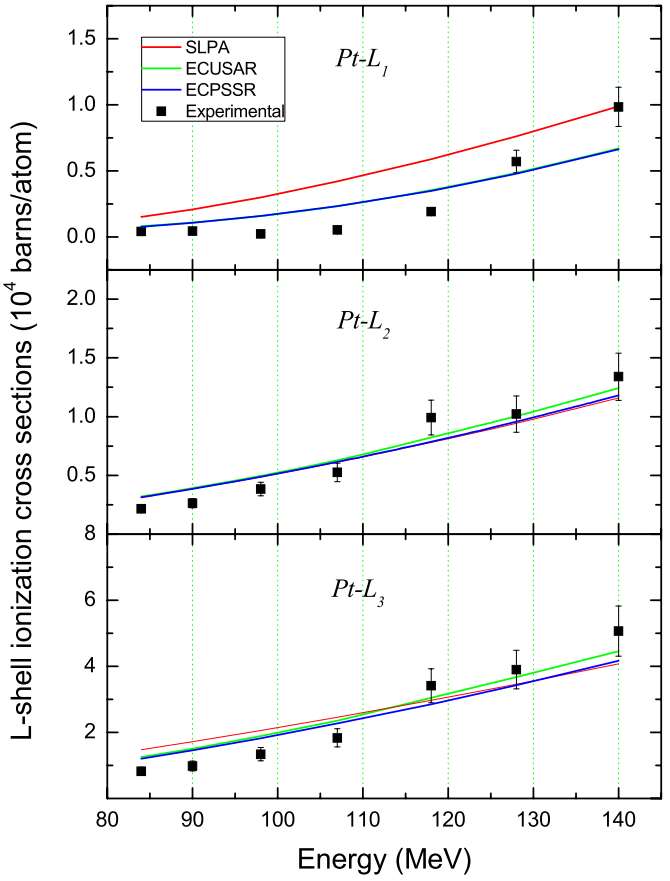

Fig. 6. Comparison of the experimental L_1, L_2, L_3 ionization cross sections for Pt induced by Si ions with different theoretical predictions: SLPA, ECUSAR, ECPSSR (details in the inset).

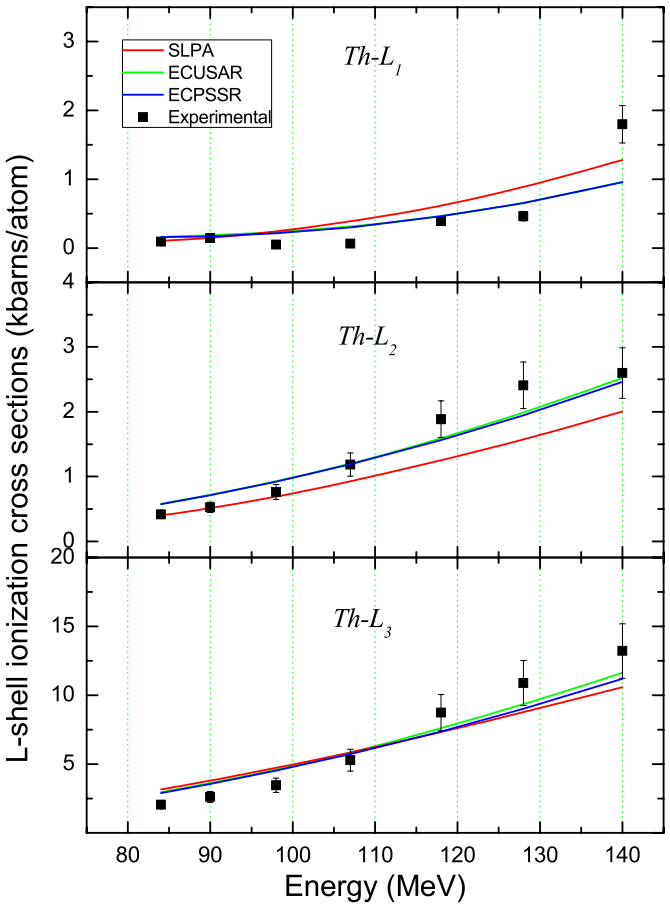

Fig. 7. Comparison of the experimental L_1, L_2, L_3 ionization cross sections for Th induced by Si ions with different theoretical predictions: SLPA, ECUSAR, ECPSSR (details in the inset).

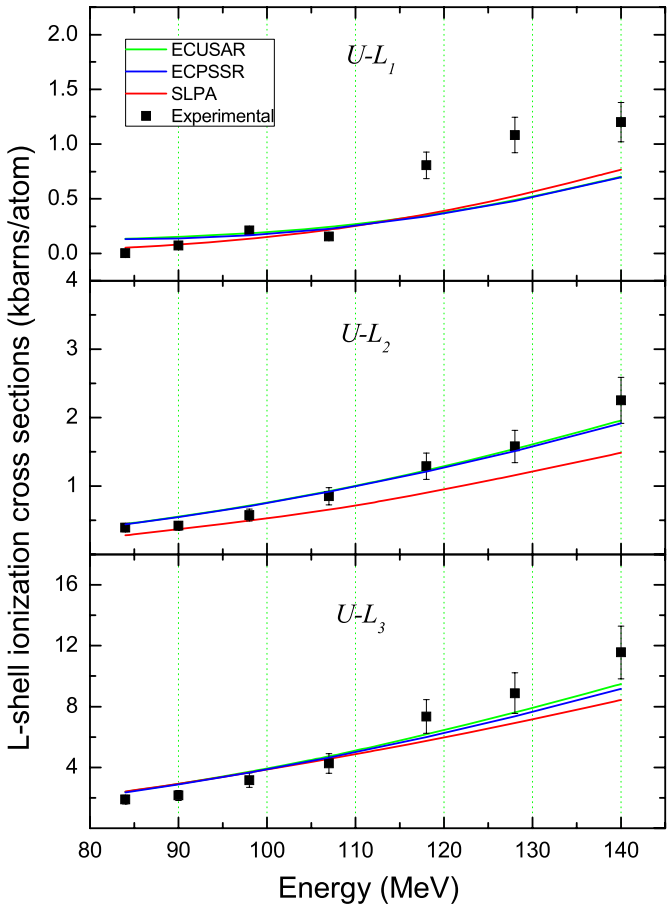

Fig. 8. Comparison of the experimental L_1, L_2, L_3 ionization cross sections for U induced by Si ions with different theoretical predictions: SLPA, ECUSAR, ECPSSR (details in the inset).

ECUSAR (Lapicki, 2002; Brandt and Lapicki, 1979, 1981; Bar-Shalom et al., 2001). We can observe in Figs. 5–8 that the experimental cross sections agree rather well with the theoretical predictions. In some cases the experiments are above the theoretical trend for E > 110 MeV, i.e. L_2 and L_3 cross sections of Ta and L_1 cross sections of U. For Ta and Pt the SLPA describes better the measurements for E > 110 MeV than for the lowest ion energies. This is reasonable because the SLPA is perturbative. However, for Th and U, it agrees well even for the lowest energies of this work, showing that the highest the target charge, the more perturbative the collision.

The comparison of the full theoretical SLPA results and the semi-empirical ECUSAR and ECPSSR is interesting because they are independent models, the former from the many-electron formalism, the latter two from the FBA and independent electron model. This comparison shows that although the SLPA results are higher than the ECUSAR for L1 cross sections, they are close to the ECUSAR ones for L2 and L3. In general, the ECPSSR predictions are lower than both, the ECUSAR and SLPA values. The ECPSSR cross sections are close to the experimental data for Ta and Pt at E < 110 MeV and for Th and U at E ≤90 MeV, but underestimate them for higher energies. This is an important concern as the ECPSSR data are used widely in PIXE codes.

6. Conclusions

The *L* x-ray production cross section of $_{73}$Ta, $_{78}$Pt, $_{79}$Th, and $_{92}$U have been measured by impact of (84–107 MeV) Si^{+8} and (118–140 MeV) Si^{+12} ions. Theoretical ionization cross sections are also presented by using the *ab initio* SLPA model together with new developments to obtain the relativistic solutions of the wave functions and binding energies for these heavy targets. The new experimental data and the SLPA results for the ionization cross sections of the L_i subshells are also compared with the known ECUSAR and ESPSSR predictions. The SLPA results are in rather good agreement with the ECUSAR ionization cross sections and also close to the experimental data as the ECUSAR. Further, the SLPA cross sections are found to be independent of the charge state of the projectile ions. This agrees with the experimental scenario only if the correct mean projectile charge state inside the target is considered, and not the outgoing charge state. This is important because the mean charge state plays a decisive role in the multiple ionization during the ion-solid collisions. We are not aware of similar observation been made in the past.

CRediT authorship contribution statement

M. Oswal: Conceptualization, Formal analysis, Investigation, Methodology, Writing - original draft. **Sunil Kumar:** Conceptualization, Formal analysis, Investigation, Methodology, Writing - original draft. **Udai Singh:** Formal analysis, Methodology, Data curation. **Shashank Singh:** Formal analysis, Methodology, Data curation. **G. Singh:** Investigation. **K.P. Singh:** Investigation, Funding acquisition, Project administration, Resources, Supervision. **D. Mehta:** Investigation, Resources, Supervision. **A.M.P. Mendez:** Investigation, Methodology, Software, Writing - original draft. **D.M. Mitnik:** Investigation, Methodology, Software, Writing - original draft. **C.C. Montanari:** Investigation, Methodology, Software, Writing - review & editing. **D. Mitra:** Formal analysis, Methodology, Validation, Writing - review & editing. **T. Nandi:** Conceptualization, Investigation, Methodology, Project administration, Software, Resources, Supervision,

Validation, Visualization, Writing - original draft, Writing - review & editing.

Declaration of competing interest

There is no **conflict of interest for this research work.**

Acknowledgements

Financial support to Mumtaz Oswal as a research fellow under a research project (KPS) from Department of Science and Technology (DST), New Delhi is highly acknowledged. Authors from Argentina acknowledge the support from CONICET, Agencia Nacional de Promoción Científicay Tecnológica, and Universidad de Buenos Aires. Authors also thank for the service of Pelletron staff for smooth operation of the machine.

Appendix A. Supplementary data

Supplementary data to this article can be found online at https://doi.org/10.1016/j.radphyschem.2020.108809.

References

Antoszewska-Moneta, M., Brzozowski, R., Moneta, M., 2015. Modification of thin films induced by slow heavy ions analysed with PIXE and SRIM. Eur. Phys. J. D. 69, 77. https://doi.org/10.1140/epjd/e2015-50629-3.

Bar-Shalom, A., Klapisch, M., Oreg, J., 2001. HULLAC, an integrated computer package for atomic processes in plasmas. J. Quant. Spectrosc. Radiat. Transf. 71, 169–188. https://doi.org/10.1016/S0022-4073(01)00066-8.

Beyer, H.F., Shevelko, V.P., 1999. Atomic Physics with Heavy Ions. Springer Berlin Heidelberg.

Brandt, W., Lapicki, G., 1979. L -shell Coulomb ionization by heavy charged particles. Phys. Rev. 20, 465–480. https://doi.org/10.1103/PhysRevA.20.465.

Brandt, W., Lapicki, G., 1981. Energy-loss effect in inner-shell Coulomb ionization by heavy charged particles. Phys. Rev. 23, 1717–1729. https://doi.org/10.1103/PhysRevA.23.1717.

Campbell, J.L., 2003. Fluorescence yields and Coster – Kronig probabilities for the atomic L subshells q. Atomic Data Nucl. Data Tables 85, 291–315. https://doi.org/10.1016/S0092-640X(03)00059-7.

Campbell, J.L., 2009. Fluorescence yields and Coster-Kronig probabilities for the atomic L subshells. Part II: the L1 subshell revisited. Atomic Data Nucl. Data Tables 95, 115–124. https://doi.org/10.1016/j.adt.2008.08.002.

Campbell, J.L., Wang, J.X., 1989. Interpolated Dirac-Fock values of L-subshell x-ray emission rates including overlap and exchange effects. Atomic Data Nucl. Data Tables 43, 281–291. https://doi.org/10.1016/0092-640X(89)90004-1.

Cantero, E.D., Fadanelli, R.C., Montanari, C.C., Behar, M., Eckardt, J.C., Lantschner, G.H., Miraglia, J.E., Arista, N.R., 2009. Experimental and theoretical study of the energy loss of Be and B ions in Zn. Phys. Rev. 79, 42904. https://doi.org/10.1103/PhysRevA.79.042904.

Chen, M.H., Crasemann, B., Mark, H., 1981. Widths and fluorescence yields of atomic L-shell vacancy states. Phys. Rev. 24, 177–182. https://doi.org/10.1103/PhysRevA.24.177.

Clementi, E., Roetti, C., 1974. Roothaan-Hartree-Fock atomic wavefunctions. Basis functions and their coefficients for ground and certain excited states of neutral and ionized atoms, Z54. Atomic Data Nucl. Data Tables 14, 177–478. https://doi.org/10.1016/S0092-640X(74)80016-1.

Crothers, D.S.F., McCann, J.F., 1984. A second-order continuum distorted-wave theory of charge transfer at high energy. J. Phys. B Atom. Mol. Phys. 17, L177–L184. https://doi.org/10.1088/0022-3700/17/6/005.

Deslattes, R.D., Kassler, E.G., Indelicato, P., De Billy, L., Lindroth, E., Anton, J., 2003. X-ray transition energies: new approach to a comprehensive evaluation. Rev. Mod. Phys. 75, 35–99. https://doi.org/10.1103/RevModPhys.75.35.

Dyson, N.A., 1990. X-rays in Atomic and Nuclear Physics, second ed. Cambridge University Presshttps://doi.org/10.1002/xrs.1300050217.

Garcia, J.D., Fortner, R.J., Kavanagh, T.M., 1973. Inner-shell vacancy production in ion-atom collisions. Rev. Mod. Phys. 45, 111–177. https://doi.org/10.1103/RevModPhys.45.111.

Gillespie, A.W., Phillips, C.L., Dynes, J.J., Chevrier, D., Regier, T.Z., Peak, D., 2015. Advances in using soft X-ray spectroscopy for measurement of soil biogeochemical processes. Adv. Agron. 133, 1–32. https://doi.org/10.1016/bs.agron.2015.05.003.

https://physics.nist.gov/cgi-bin/Xcom/xcom3_1.

Johansson, T.B., Akselsson, R., Johansson, S.A.E., 1970. X-ray analysis: elemental trace analysis at the 10-12 g level. Nucl. Inst. Methods. B. 84, 141–143. https://doi.org/10.1016/0029-554X(70)90751-2.

Kadhane, U., Montanari, C., Tribedi, L., 2003. K-shell processes in heavy-ion collisions in solids and the local plasma approximation. Phys. Rev. 67, 1–7. https://doi.org/10.1103/PhysRevA.67.032703.

Klapisch, M., 1971. A program for atomic wavefunction computations by the parametric potential method, Comput. Phys. Commun. 2, 239–260. https://doi.org/10.1016/0010-4655(71)90001-4.

Krause, M.O., 1979. Atomic radiative and radiationless yields for K and L shells. J. Phys. Chem. Ref. Data 8, 307–327. https://doi.org/10.1063/1.555594.

Kumar, S., Singh, U., Oswal, M., Singh, G., Singh, N., Mehta, D., Nandi, T., Lapicki, G., 2017. L shell x ray production in high-Z elements using 4–6 MeV/u fluorine ions. Nucl. Instrum. Methods Phys. Res. Sect. B Beam Interact. Mater. Atoms 395, 39–51. https://doi.org/10.1016/j.nimb.2017.01.044.

Lamour, E., Fainstein, P.D., Galassi, M., Prigent, C., Ramirez, C.A., Rivarola, R.D., Rozet, J.-P., Trassinelli, M., Vernhet, D., 2015. Phys. Rev. A 92, 042703. https://doi.org/10.1103/PhysRevA.92.042703.

Lapicki, G., 2002. The status of theoretical L-subshell ionization cross sections for protons. Nucl. Instrum. Methods Phys. Res. Sect. B Beam Interact. Mater. Atoms 189, 8–20. https://doi.org/10.1016/S0168-583X(01)00987-9.

Lapicki, G., Mehta, R., Duggan, J.L., Kocur, P.M., Price, J.L., McDaniel, F.D., 1986. Multiple outer-shell ionization effect in inner-shell x-ray production by light ions. Phys. Rev. 34, 3813–3821. https://doi.org/10.1103/PhysRevA.34.3813.

Lapicki, G., Ramana Murty, G.A.V., Naga Raju, G.J., Reddy, B.S., Reddy, S.B., Vijayan, V., 2004. Effects of multiple ionization and intrashell coupling in L -subshell ionization by heavy ions. Phys. Rev. 70, 062718. https://doi.org/10.1103/PhysRevA.70.062718.

Levine, Z.H., Louie, S.G., 1982. New model dielectric function and exchange-correlation potential for semiconductors and insulators. Phys. Rev. B 25, 6310–6316. https://doi.org/10.1103/PhysRevB.25.6310.

Mehta, R., Duggan, J.L., McDaniel, F.D., McNeir, M.R., Yu, Y.C., Marble, D.K., Lapicki, G., 1993. L-shell X-ray production cross sections for 29Cu, 31Ga, 32Ge, 35Br, 39Y, 60Nd, 64Gd, 67Ho, 70Yb, 79Au, and 82Pb for 2-25 MeV carbon ions. Nucl. Instrum. Methods B. 79, 175–178. https://doi.org/10.1016/0168-583X(93)95318-Y.

Montanari, C.C., Miraglia, J.E., 2013. Theory of Heavy Ion Collision Physics in Hadron Therapy. https://doi.org/10.1016/B978-0-12-396455-7.00006-6.

Montanari, C.C., Miraglia, J.E., 2017a. Low- and intermediate-energy stopping power of protons and antiprotons in solid targets. Phys. Rev. 96, 012707. https://doi.org/10.1103/PhysRevA.96.012707.

Montanari, C.C., Miraglia, J.E., 2018b. Ionization probabilities of Ne, Ar, Kr, and Xe by proton impact for different initial states and impact energies. Nucl. Instrum. Methods Phys. Res. Sect. B Beam Interact. Mater. Atoms 407, 236–243. https://doi.org/10.1016/j.nimb.2017.07.001.

Montanari, C.C., Mitnik, D.M., Miraglia, J.E., 2011. A collective model for inner shell ionization of very heavy targets. Radiat. Eff. Defect Solid 166, 338–345. https://doi.org/10.1080/10420150.2011.572284.

Naga Raju, G.J., V Ramana Murty, G.A., Seetharami Reddy, B., Seshi Reddy, T., Lakshminarayana, S., Bhuloka Reddy, S., 2004. Multiple ionization effects on L X-ray intensity ratios in Hf, Ta, Re, Ir, Pt, Au and Pb due to proton bombardment at energies 1-5 MeV. Eur. Phys. J. D. 30, 171–179. https://doi.org/10.1140/epjd/e2004-00085-3.

Nandi, T., Sharma, P., Kumar, P., 2018. Unusual charge exchange by swift heavy ions at solid surfaces. https://www.researchgate.net/publication/327573235_Unusual_charge_exchange_by_swift_heavy_ions_at_solid_surfaces.

Oreg, J., Goldstein, W.H., Klapisch, M., Bar-Shalom, A., 1991. Autoionization and radiationless electron capture in complex spectra. Phys. Rev. 44, 1750–1758. https://doi.org/10.1103/PhysRevA.44.1750.

Oswal, M., Kumar, S., Singh, U., Singh, G., Singh, K.P., Mehta, D., Mitnik, D., Montanari, C.C., Nandi, T., 2018. L x-ray production cross sections in high-Z atoms by 3–5 MeV/u silicon ions. Nucl. Instrum. Methods Phys. Res. Sect. B Beam Interact. Mater. Atoms 416, 110–118. https://doi.org/10.1016/J.NIMB.2017.11.025.

Pajek, M., Banaś, D., Semaniak, J., Braziewicz, J., Majewska, U., Chojnacki, S., Czyżewski, T., Fijał, I., Jaskóła, M., Glombik, A., Kretschmer, W., Trautmann, D., Lapicki, G., Mukoyama, T., 2003. Multiple ionization and coupling effects in L -subshell ionization of heavy atoms by oxygen ions. Phys. Rev. 68, 022705. https://doi.org/10.1103/PhysRevA.68.022705.

Richard, P., 1975. Ion-atom collisions. In: Atomic Inner-Shell Processes. Academic Press, New York. https://doi.org/10.1007/978-1-4613-2417-1.

Satoh, T., 2015. Development of particle induced X-ray emission-computed tomography in Takasaki advanced radiation research institute, Japan atomic energy agency. Int. J. PIXE 25, 147–152. https://doi.org/10.1142/S0129083515500151.

Schiwietz, G., Grande, P.L., 2001. Improved charge-state formulas. Nucl. Instrum. Methods Phys. Res. Sect. B Beam Interact. Mater. Atoms 175–177, 125–131. https://doi.org/10.1016/S0168-583X(00)00583-8.

Scofield, J.H., 1974. Relativistic hartree-slater values for K and L X-ray emission rates. Atomic Data Nucl. Data Tables 14, 121–137. https://doi.org/10.1016/S0092-640X(74)80019-7.

Sharma, P., Nandi, T., 2016. Experimental evidence of beam-foil plasma creation during ion-solid interaction. Phys. Plasmas 23, 083102. https://doi.org/10.1063/1.4960042.

Singh, Y.P., Mitra, D., Tribedi, L.C., Tandon, P.N., 2000. L-subshell ionization of Bi, Au, and Yb induced by F ions at intermediate velocities. Phys. Rev. 63, 012713. https://doi.org/10.1103/PhysRevA.63.012713.

Williams, G.P., 1992. Electron binding energies of the elements. CRC Handb. Chem. Physics, 92nd Ed. Sect. 10, 221–226.